Solidification of a simple liquid near wall in high-speed shear flows

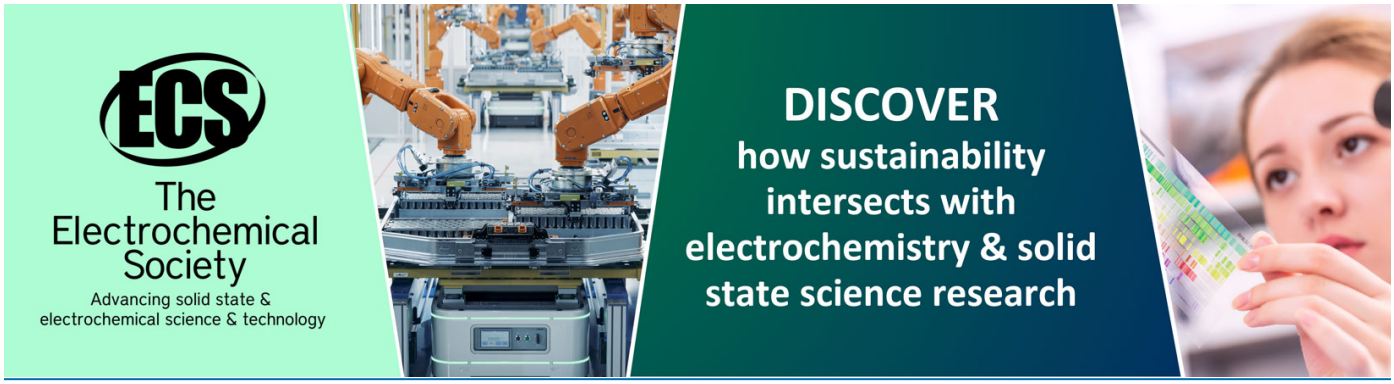

IOP Conf. Series: Journal of Physics: Conf. Series **1136** (2018) 012027 doi:10.1088/1742-6596/1136/1/012027

Solidification of a simple liquid near wall in high-speed shear flows

Shugo YASUDA and Ryo OOKAWA

Graduate School of Simulation Studies, University of Hyogo, Kobe 6500047, Japan

E-mail: yasuda@sim.u-hyogo.ac.jp

Abstract. The viscous-heating-induced solidification of a Lennard-Jones fluid near wall in high-speed shear flows is discovered by the molecular-dynamics simulation. The solidification is characterized by a non-dimensional parameter defined by the ratio of the viscous heating to the thermal conductivity of the fluid and is observed only when the channel width is sufficiently large, where the macroscopic transport becomes significant. Thus, the solidification is thought to be due to the macroscopic heat and mass transport induced by the *viscous heating* generated in the fluid regime by the high-speed shear flow. Unexpectedly, shear bands also appear near wall when the solidification occurs.

1. Introduction

Lubrication is a fundamental and classical problem in the fluid dynamics. However, the behaviors become very complicated in complex mechanical systems and extreme environments, where the complex rheology of structured fluid, the chemical reaction at complex interface, and the phase transition in high-speed lubrication are mainly concerned.[1, 2, 3] Computer simulations for those complicated lubrication systems are still challenging and important both from academic and practical points of views.

The computational fluid dynamics (CFD) approaches based on the macroscopic models are useful unless the constitutive relations between macroscopic quantities are prescribed. However, the constitutive relations are unknown for the complex fluids in general.

The molecular-dynamics (MD) simulation is useful even for the complex fluids which cannot be addressed by the CFD approach because any complicated phenomena are autonomously reproduced once their molecular models are appropriately specified in principle.[4, 5, 6]

In this paper, we carry out the large-scale MD simulation of the high-speed lubrication of a Lennard-Jones fluid, which may involve the phase transition. Apart from the conventional MD approaches utilizing the thermostat algorithms to artificially control the fluid temperature, our MD simulation concerns the *viscous heating* generated by the high-speed shear flows as they are naturally observed in real lubrication systems.

The MD simulations for the thermal lubrication in nano channel have been studied by various researchers.[7, 8, 9, 10] However, in this study, we consider the channels which widen much larger than the molecular scale, where the macroscopic transport becomes important. Thus, our study is concerned with the thermal lubrication which is practically important in micro-mechanical systems.

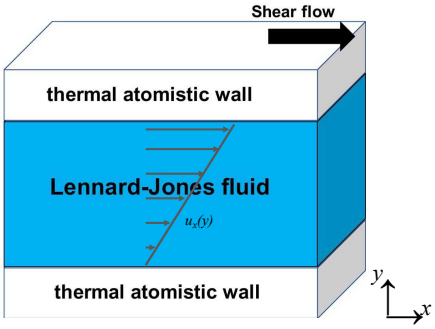

Figure 1. The schematic of the problem. The LJ fluid is sandwiched by atomistic walls kept at a constant temperature T^w. The boundary-driven shear flows are considered in this paper. The x-axis is set in the flow direction and the y-axis is set in the direction perpendicular to the parallel walls. In the x-direction, the periodic boundary condition is considered. The linear flow velocity profile for the iso-thermal fluid is also drawn in the figure.

Incidentally, the drawback of MD simulation comparing to the CFD approach is the huge computational cost. To overcome this difficulty, the development of the multiscale method is currently very active research field.[11, 12, 13, 14, 15] We have also recently developed a multiscale method called Synchronized Molecular-Dynamics (SMD) method and applied it to the thermal lubrication of polymeric fluid with a uniform density, where the mass transports are neglected.[16, 17, 18, 19, 20, 21, 22] Although the multiscale approaches are powerful and promising for complex fluids, in order to further develop the multiscale methods, we need more first-principle results obtained by the full MD simulation. Thus, in this paper, we concern the full MD simulation which can reproduce the full macroscopic transport, i.e., the mass, momentum, and heat transfers, autonomously.

2. Problem and model

We consider a Lennard-Jones (LJ) fluid between parallel plates, which is shown in Fig. 1. The fluid domain is ranged over $y \in (0, H)$ and the wall domains are ranged over $y \in [-W, 0]$ (the lower wall) and $y \in [H, H+W]$ (the upper wall). Both of the fluid and walls are composed of LJ particles which interact each other via the LJ potential

$$U(r) = \begin{cases} 4\varepsilon \left[\left(\frac{\sigma}{r}\right)^{12} - \left(\frac{\sigma}{r}\right)^{6} \right], & (0 < r < r_c), \\ 0, & (r_c \le r). \end{cases} \tag{1}$$

Here, r_c is the cut-off parameter and ε and σ are the units of energy and length of the LJ particles, respectively. The wall and fluid particles are considered to be the same in the size and mass.

The wall particles are also connected to the face-centered cubic (FCC) lattice structure $\{\boldsymbol{r}_i^w\}$ by a spring potential, and the temperature of wall particles is kept at a constant T^w by the Langevin thermostat algorithm.

Thus, the dynamics of LJ particles are described as

$$m\ddot{\boldsymbol{r}}_i(t) = -\sum_j \frac{\partial U(|\boldsymbol{r}_{ij}|)}{\partial \boldsymbol{r}_{ij}}, \tag{2}$$

for the fluid particles (i.e., $r_{y_i} \in (0, H)$), and

$$m\ddot{\boldsymbol{r}}_i(t) = -\sum_j \frac{\partial U(|\boldsymbol{r}_{ij}|)}{\partial \boldsymbol{r}_{ij}} - k_s(\boldsymbol{r}_i - \boldsymbol{r}_i^w) - \gamma \dot{\boldsymbol{r}}_i + \boldsymbol{R}(t), \tag{3}$$

Boundary-driven		
Case	H	V^w
A	56	3.0
B	168	1.0
C	252	3.0
D	756	1.0
E	67	2.5
F	84	2.0
G	302	2.0
H	378	2.0
I	112	1.5
J	168	3.0

Table 1. Parameter values used in the boundary-driven shear flows. In this proceedings, only the results of Case C are mainly presented.

for the wall particles (i.e., $r_{y_i} \in [-W, 0] \cup [H, H+W]$), where $R_\alpha(t)$ ($\alpha = x, y, z$) is the white Gaussian noise, which satisfies,

$$< R_\alpha(t) R_\beta(t-s) >= 2mk_B T^w \gamma \delta_{\alpha\beta} \delta(s). \tag{4}$$

Here, $\boldsymbol{r}_i$ represents the position of the ith particle, $\boldsymbol{r}_{ij}$ is defined as $\boldsymbol{r}_{ij} = \boldsymbol{r}_i - \boldsymbol{r}_j$, m is the mass of LJ particle, k_s is the spring constant, γ is the damping coefficient, and k_B is the Boltzmann constant. Note that the summation $\sum_j$ counts for both of fluid- and wall-particles.

The cut-off length $r_c = 2.8$, spring constant $k_s = 10$ and damping coefficient $\gamma = 0.1$ are fixed. Hereafter, we measure the quantities by the units of mass m, energy ε, length σ, and time $\tau = \sqrt{m\sigma^2/\varepsilon}$.

We remark that the temperature of the fluid is not artificially controlled by any thermostat algorithms but varies spatially and temporally due to the macroscopic transport of mass, momentum, and heat between the parallel plates walls with a constant temperature T^w. We also note that the temperature of the moving wall (the upper wall) is controlled only by the y and z components of thermal velocity while the x velocity is given by a constant velocity $v_x = V^w$.

The LJ fluid is initially in a uniform liquid state whose density $\rho_0 = 0.844$ and temperature $T_0 = 0.722$ are fixed near the triple point of the LJ potential. This initial state of LJ fluid is produced by a long-time quiescent MD simulation of the system shown in Fig. 1.

The width of channel H, which is shown in Table 1, is much larger than the molecular size. Thus, the inhomogeneous distributions of macroscopic quantities, e.g., density, velocity, and temperature, may be created due to the macroscopic transport of mass, momentum, and heat between the parallel plates.

3. Results

The lengths of simulation box in x- and z-directions, $L_x = L_z = 16.8$ are fixed while the width of channel H varies as shown in Table 1. The thickness of slab wall $W \simeq 4.1$ is fixed. Thus, for example, the number of particles is about 6.2×10^4 for Case C. The MD simulations are performed by using the LAMMPS software package [23, 24], in which Eq.(2) is time-integrated by the velocity-verlet method with the time-step size $\Delta t = 0.005$.

The channel width H is uniformly divided into 20 bins and, in each bin, the local macroscopic quantities, i.e., density ρ, flow velocity u_x, temperature T, and stress $p_{\alpha\beta}$ are calculated in the stationary state after a long time τ_0 has passed (i.e., $\tau_0 = 1.53 \times 10^8 \Delta t$ is taken for Case D in

Table 1 and $\tau_0 = 6 \times 10^7$ for the other cases). The local macroscopic quantities are also time-averaged in each 100,000 time-steps interval, in which instantaneous macroscopic quantities are sampled at every 10 time steps (i.e., 10,000 samples are averaged for each local macroscopic quantity). The standard deviations of the instantaneous local macroscopic quantities are at most 0.0044 for the density, 0.023 for the velocity, 0.018 for the temperature, and 0.15 for the normal stress. See also Fig. 2.

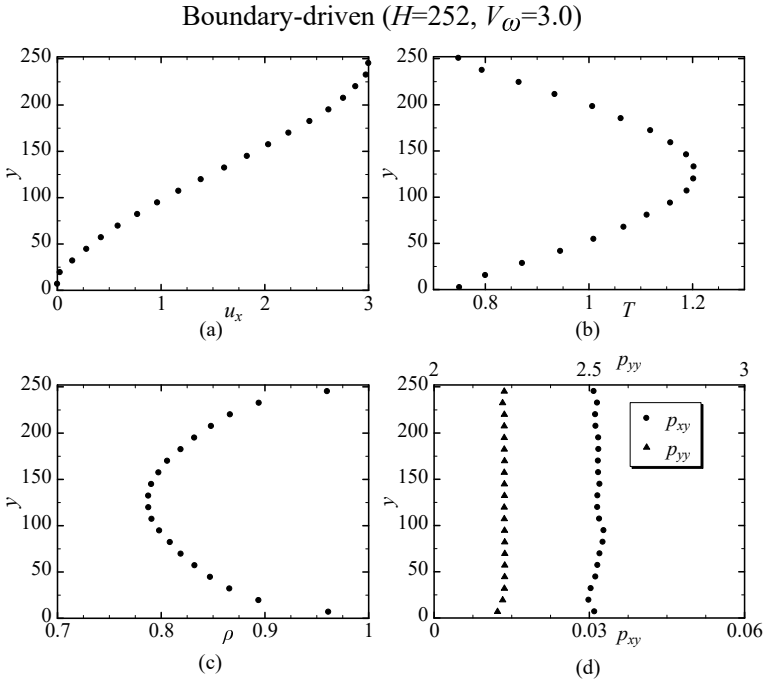

Figure 2. The spatial distributions of velocity (a), temperature (b), density (c), and shear and normal stresses (d) for Case C in Table 1. The standard deviations of the instantaneous local macroscopic quantities are at most 0.023 for u_x, 0.018 for T, 0.0044 for ρ, and 0.15 for p_{yy}.

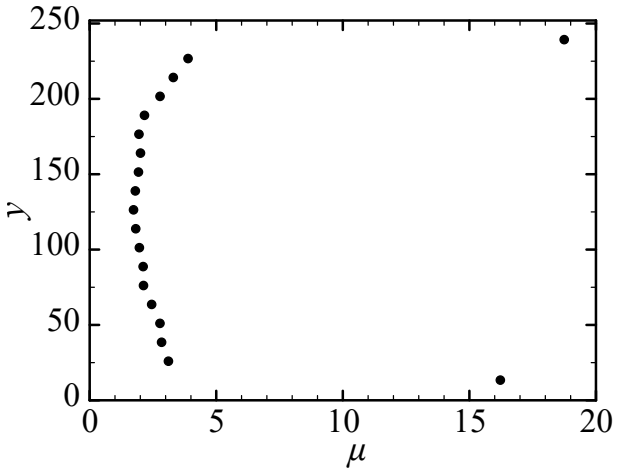

Figure 3. The spatial distribution of local viscosity μ, which is calculated as the ratio of local shear stress p_{xy} to the local share rate $\dot{\gamma}$ $(=\partial u_x/\partial y)$, i.e., $\mu = p_{xy}/\dot{\gamma}$, for Case C in Table 1.

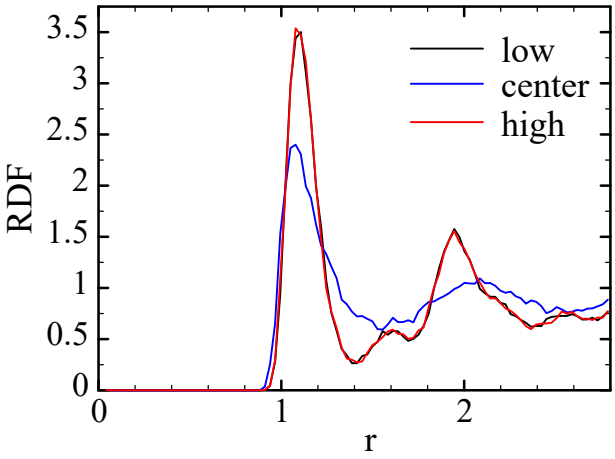

Figure 4. The radial distribution functions (RDF) in the upper, middle, and lower regions at time $t = \tau_0$. The small second peaks of RDF in the upper and bottom regions correspond to the characteristic of the RDF in FCC lattice structure. The local density in the upper and lower regions (solid phase) is $\rho = 0.96$ while that in the middle region is $\rho = 0.79$. See also Fig. 2(c) for the local density profile.

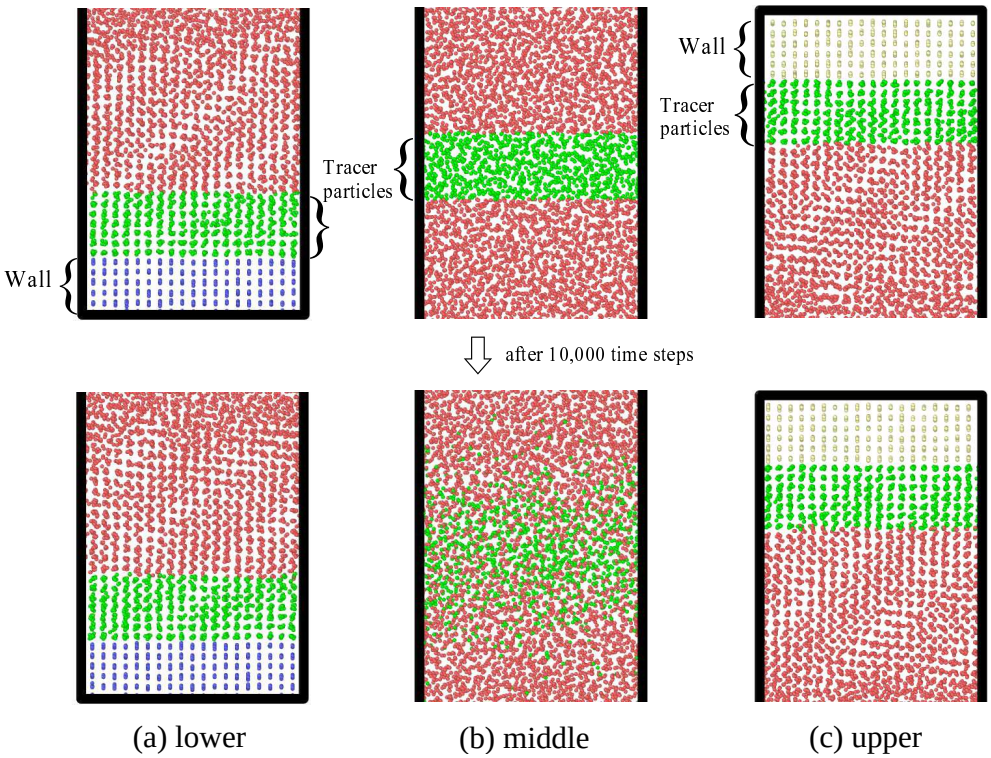

Figure 5. The snapshots of molecules contained in the lower (a), middle (b), and upper (b) regions at two different time steps. The movements of colored molecules in upper figures after 10,000 time steps are shown in the lower figures. The shear banding layer near walls broadens out about 15σ's thickness in Figs. (a) and (c).

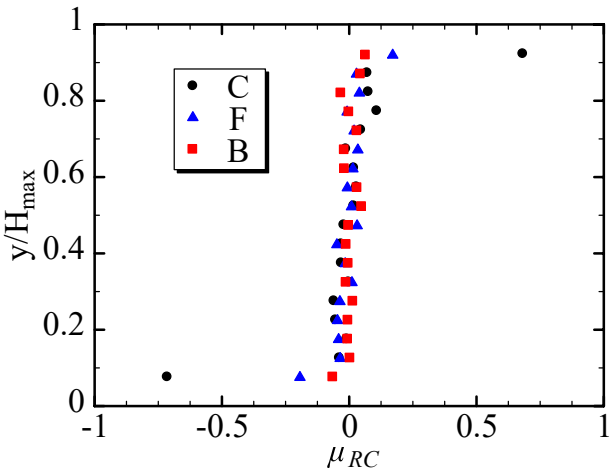

Figure 6. The spatial distributions of the rate of change of local viscosity defined by Eq. 5 for case C, F, and B in Table 1.

Figures 2 and 3 show the spatial distributions of local macroscopic quantities (i.e., velocity, temperature, density, and stress) and local viscosity for Case C in Table 1, respectively.

In Fig. 2, it is seen that both of the normal and shear stresses, p_{yy} and p_{xy} are uniformly distributed between the upper and bottom walls. This confirms that the local stresses are balanced so that the flow velocity is in the stationary state. On the other hand, the other macroscopic quantities vary largely between the walls. The temperature increases in the middle region due to the viscous heating while the temperatures near walls are kept at constant $T \simeq T_w$. Thus, the local density remarkably increases in the vicinity of walls.

Interestingly, the velocity gradient becomes much smaller in the vicinity of walls, where the local viscosities are remarkably increased. See Fig. 3. Thus, the thickening of local viscosity occurs in the vicinity of walls. In order to investigate the local material state, we also calculate the radial distribution function (RDF) of LJ particles included in the upper, lower, and center bins in Fig. 4.

Surprisingly, we can find the solidification of LJ fluid in the vicinity of walls in Fig. 4. The RDF in the upper and lower regions exhibit the second peak around $r \simeq 1.7$, which is the characteristic of the FCC lattice structure, while that in the center bin does not show the second peak but is similar to that of the liquid structure.

The solidification in the vicinity of wall is also confirmed by the movements of tracer particles in Fig. 5. Remarkably, the tracer particles in the lower region do not diffuse in the lateral direction (y direction) but are confined in the vicinity of wall while those in the middle region diffuse in the lateral direction as liquid molecules.

Furthermore, unexpectedly, we can observe shear bands in the vicinities of walls. The shear banding layers broaden out about 15σ's thickness over the walls, where the particles are closely packed because they are strongly pushed toward the wall by the dilation of fluid in the middle region due to the viscous heating.

4. Discussion

In this section, we discuss the non-dimensional parameter which is relevant to the solidification mechanism. We classify the state of LJ fluid near wall by using the rate of change of local viscosity defined by

$$\mu_{RC} = \frac{\partial \log \mu}{\partial y}. \tag{5}$$

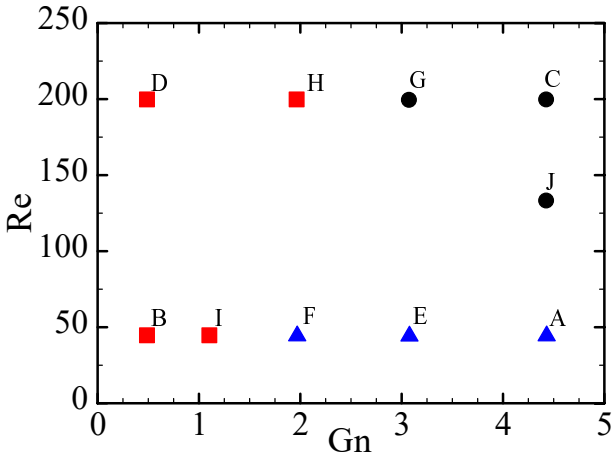

Figure 7. The diagram of the local state near wall in terms of two non-dimensional parameters defined by Eqs. (6) and (7). The results for the parameter sets in Table 1 are shown. The symbols ◯, △, and □ represent the solid, semi-solid, and liquid state, respectively.

Figure 6 shows the distributions of μ_{RC} for case C, F, and B in Table 1. The rate of change of viscosity is quite small, $|\mu_{RC}| \ll 1$ in the region except for the vicinity of walls. Remarkably, it exhibits jumps only in the vicinity of walls for Case C, where the solidification occurs.

We qualitatively distinguish the states of LJ fluid near wall for all cases shown in Table 1 by using the maximum values of $|\mu_{RC}|$; say, the solid state for $|\mu_{RC}| \geq 0.4$, semi-solid state for $0.1 < |\mu_{RC}| < 0.4$, and liquid state for $|\mu_{RC}| \leq 0.1$ in this study.

Figure 7 is the diagram of state near wall in terms of two non-dimensional parameters defined as,

$$Re = \frac{H}{\mu_0/\rho_0 V_M} \frac{\rho_0 V_M H}{\mu_0} \propto V_M H, \tag{6}$$

$$Gn = \frac{\mu_0 V_M^2/H^2}{\lambda_0 \Delta T/H^2} = \frac{\mu_0 V_M^2}{\lambda_0 \Delta T} \propto V_M^2. \tag{7}$$

Here V_M is the maximum flow velocity, ΔT is the characteristic temperature difference, and μ_0 and λ_0 are the viscosity and thermal conductivity of LJ fluid in the initial state, which is calculated as $\mu_0 = 3.2$ and $\lambda_0 = 6.5$, respectively, by the equilibrium MD simulation. We also remark that the choice of ΔT is arbitrary and $\Delta T = 1$ is fixed in this paper.

The first non-dimensional parameter Re, the Reynolds number measures the relative width of channel H to viscous length $\mu_0/(\rho_0 V_M)$ and the second non-dimensional parameter Gn measures the relative effect of viscous heating to thermal conductivity.

It is seen that Gn is more relevant to characterize the transition from liquid to solid states than Re. However, the solid states do not appear at small Reynolds numbers even if Gn is large. The solidification only occurs when the channel width is sufficiently large. This fact may indicate that the large system size is required for the LJ fluid to be segregated in two different phases.

5. Concluding remarks and perspective

We discovered a novel solidification and shear banding phenomenon near wall occurring in the high-speed shear flow between the parallel plates by the molecular-dynamics simulation. The solidification and shear banding near wall is only observed when the channel width is sufficiently large, where the highly-inhomogeneous distributions of macroscopic quantities

are created between the walls. The phase transition near wall is characterized by the non-dimensional parameter Gn, which measures the relative effect of the viscous heating to the thermal conductivity of LJ fluid between walls. Thus, the solidification near wall is thought to be due to the heat and mass transport induced by the viscous heating in the fluid regime.

In order to elucidate the solidification mechanism more clearly, the effect of the lattice structure of wall atoms will be important in the future work.

The solidification near wall related to the viscous heating has also been discussed in Ref. [25], where the solid-like layering near wall was discovered in a two-dimensional nanochannel. Actually, in the paper, the solid-like layering is much thinner than that in Fig. 5 and the effect of the macroscopic transport is not clearly distinguishable from the effect of the wall atoms because the channel width is only 48σ. However, the solidification mechanism seems to be similar to that observed in the present paper.

The MD simulation can autonomously reproduce the heat-generating shear flows coupling with phase transition as they may occur in real high-speed lubrication systems. Importantly, this study demonstrates that the application of MD simulation to fluid dynamics problem can unveil a hidden physical phenomenon, which cannot be ever addressed by any conventional CFD approaches, even in the fundamental flow problems.

Acknowledgements
This study was financially supported by JSPS KAKENHI Grant Number 16K17554 and 17H01083.

References

[1] R. B. Bird, R. C. Armstrong, and O. Hassager, *Dynamics of polymeric liquids* Vol. 1 (John Wiley and Sons, New York, 1987).
[2] Y. Hori, *Hydrodynamics lubrication* (Springer-Verlag, Tokyo, 2006).
[3] C. J. Pipe, T. S. Majmudar, and G. H. McKinley, "High shear rate viscometry", Rheol Acta **47**, 621 (2008).
[4] M. P. Allen and D. J. Tildesley, *Computer Simulation of Liquids*, (Oxford University Press, New York, 1989).
[5] D. J. Evans and G. Morris, *Statistical mechanics of nonequilibrium liquids*, (Cambridge university press, New York, 2008).
[6] G. E. Karniadakis, A. Beskok, and N. Aluru, *Microflows and nanoflows: fundamentals and simulation* (Springer, New York, 2005).
[7] R. Khare, J. de Pablo, and A. Yethiraj, "Molecular simulation and continuum mechanics study of simple fluids in non-isothermal planar couette flows", J. Chem. Phys. **107**, 2589 (1997).
[8] J. S. Hansen and J. T. Ottesen, "Molecular dynamics simulations of oscillatory flows in microfluidic channels", Microfluid Nanofluid **2**, 301 (2006).
[9] B. H. Kim, A. Beskok, and T. Cagin, "Viscous heating in nanoscale shear driven liquid flows", Microfluid Nanofluid **9**, 31 (2010).
[10] J. Ghorbanian and A. Beskok, "Temperature profiles and heat fluxes observed in molecular dynamics simulations of force-driven liquid flows", Phys. Chem. Chem. Phys. **19**, 10317 (2017).
[11] W. E and B. Engquist, "The heterogeneous multi-scale methods", Commun Math. Sci. **1**, 87 (2003).
[12] I. G. Kevrekidis, C. W. Gear, J. M. Hyman, P. G. Kevrekidis, O. Runborg, and C. Theodoropoulos, "Equation-free, coarse-grained multiscale computation: enabling microscopic simulations to perform system-level analysis", Comm. Math. Sci. **1**, 715 (2003).
[13] W. Ren and W. E, "Heterogeneous multiscale method for the modeling of complex fluids and micro-fluidics", J. Comput. Phys. **204**, 1 (2005).
[14] I. G. Kevrekidis and G. Samaey, "Equation-free multiscale computation: algorithms and applications", Annu. Rev. Phys. Chem. **60**, 321 (2009).
[15] M. K. Borg, D. A. Lockerby, and J. M. Reese, "Multiscale method for micro/nano flows of high aspect ration", J. Comput. Phys. **233**, 400 (2013).
[16] S. Yasuda and R. Yamamoto, "A model for hybrid simulation of molecular dynamics and computational fluid dynamics", Phys. Fluids **20**, 113101 (2008).
[17] S. Yasuda and R. Yamamoto, "Rheological properties of polymer melt between rapidly oscillating plates: an application of multiscale modeling", Europhys. Lett. **86**, 18002 (2009).

[18] S. Yasuda and R. Yamamoto, "Multiscale modeling and simulation for polymer melt flows between parallel plates", Phys. Rev. E **81**, 036308 (2010).
[19] S. Yasuda and R. Yamamoto, "Dynamic rheology of a supercooled polymer melt in nonuniform oscillating flows between rapidly oscillating plates", Phys. Rev. E **84**, 031501 (2011).
[20] T. Murashima, S. Yasuda, T. Taniguchi, and R. Yamamoto, "Multiscale modeling for polymeric flow: particle-fluid bridging scale methods", J. Phys. Soc. Jpn. **82**, 012001 (2013).
[21] S. Yasuda and R. Yamamoto, "Synchronized molecular-dynamics simulation via macroscopic heat and momentum transfer", Phys. Rev. X **4**, 041011 (2014).
[22] S. Yasuda and R. Yamamoto, "Synchronized molecular-dynamics simulation for the thermal lubrication of a polymeric liquid between parallel plates", Comput. Fluids **124**, 185 (2016).
[23] S. Plimpton, "Fast parallel algorithms for short-range molecular dynamics", J. Comput. Phys., **117**, 1–19 (1995).
[24] http://lammps.sandia.gov
[25] M. Priya and Y. Rabin, "Molecular dynamics simulations of shear-induced thermophoresis and non-Newtonian flow in compressible fluids", arXiv: 1703.1046.